Energy levels and intensity parameters of Ho^{3+} ions in $GdLiF_4$, $YLiF_4$ and $LuLiF_4$

2005 J. Phys.: Condens. Matter 17 7643

(http://iopscience.iop.org/0953-8984/17/48/016)

INSTITUTE OF PHYSICS PUBLISHING JOURNAL OF PHYSICS: CONDENSED MATTER

J. Phys.: Condens. Matter **17** (2005) 7643–7665 doi:10.1088/0953-8984/17/48/016

Energy levels and intensity parameters of Ho^{3+} ions in $GdLiF_4$, $YLiF_4$ and $LuLiF_4$

Brian M Walsh, Gary W Grew and Norman P Barnes

NASA Langley Research Center, Hampton, VA 23681, USA

Received 6 July 2005, in final form 17 October 2005
Published 11 November 2005
Online at stacks.iop.org/JPhysCM/17/7643

Abstract

While the energy levels in Ho:YLF have been measured previously, they have not been as thoroughly investigated in the isomorphs, Ho:LuLF and Ho:GdLF. We report here the measurement of the energy levels of the trivalent lanthanide Ho^{3+} in $GdLiF_4$ (GdLF), $YLiF_4$ (YLF), and $LuLiF_4$ (LuLF). The measurement of the energy levels of Ho:YLF, although they have been measured before, are repeated here for self-consistent comparison to Ho:LuLF and Ho:GdLF. The Stark split levels for the first ten Ho manifolds in these materials have been measured, and the results have been fitted to a free-ion plus crystal-field Hamiltonian to generate a theoretical set of energy levels. Crystal-field parameters were varied to determine the best fit between experimental and theoretical energy levels. The energy levels of Ho:GdLF and Ho:LuLF are seen to be very similar to those in Ho:YLF. However, subtle changes resulting from replacing Y^{3+} with Gd^{3+} or Lu^{3+} in the fluoride crystal $YLiF_4$ result in shorter transition wavelengths in GdLF and longer transition wavelengths in LuLF. This has implications for Ho $^5I_7 \rightarrow {}^5I_8$ lasers operating at $\sim$2.0 μm. The energy levels for Ho:GdLF and Ho:LuLF determined here indicate that Ho:GdLF will have a larger lower laser level thermal population than Ho:YLF, while Ho:LuLF lasers will have a smaller lower laser level thermal population than Ho:YLF. This is consistent with the larger Stark splitting associated with the larger host ions that Ho substitutes for in these lithium fluoride materials. The intensity parameters are also determined from a Judd–Ofelt analysis and used to calculate radiative lifetimes and branching ratios for the first ten manifolds in Ho:GdLF, Ho:YLF and Ho:LuLF.

1. Introduction

There continues to be interest in Tm sensitized Ho luminescence in various host materials for producing 2 μm lasers. Solid state lasers operating around 2.0 μm are useful for a number of applications including lidar for heterodyne measurement of wind velocity, eye safe range-finding, medical applications and as sources for mid-infrared optical parametric oscillators.

Tm:Ho materials have remained the material of choice for 2.0 μm lasers. Tm:Ho:YLF has been an especially popular material due to its thermal and physical properties. Recently, Tm:Ho:LuLF has gained popularity as well. The improved performance of Tm:Ho:LuLF over Tm:Ho:YLF for Ho $^5I_7 \rightarrow {}^5I_8$ laser action at $\sim$2.0 μm was predicted in 1994 [1] and experimentally validated in 1997 [2] by researchers at NASA Langley Research Center in Hampton, VA. Recently, researchers at the Institute for Materials Research in Sendai, Japan have published diode side-pumped studies [3] validating these earlier studies. A number of other studies concerning 2 μm laser action in Tm:Ho:LuLF by Sudesh [4–7] and Petros [8, 9] have recently appeared in the literature. The interest in Tm:Ho:LuLF and its co-doped relative Tm:Ho:LuLF for 2 μm lasers has prompted a need for more information concerning Ho:LuLF.

For quasi-four-level lasers, that is, lasers which have a finite Boltzmann thermal population in the lower laser level, such as 2.0 μm Tm:Ho lasers, the crystal-field splitting of the Ho $^5I_8$ ground state determines the lower laser level population. A larger lower laser manifold splitting is beneficial in reducing the lower laser level thermal population, which benefits population inversion. In order to calculate the lower laser level population, the energy levels must be known. In addition, the energy levels are useful for determining potential laser wavelengths operating on manifolds other than the $^5I_7 \rightarrow {}^5I_8$ transition as well as determining potential energy transfer processes. So, an examination of the energy levels of Ho:GdLF and Ho:LuLF, both isomorphs of Ho:YLF, would seem to be of interest to researchers utilizing Ho^{3+} ions in GdLF and LuLF.

2. The host materials GdLF, YLF and LuLF

Lutecium lithium fluoride, $LuLiF_4$ (LuLF) and gadolinium lithium fluoride, $GdLiF_4$ (GdLF) are scheelite isostructures similar to $YLiF_4$ (YLF). These materials are simple fluoride crystals with a tetragonal scheelite structure (space group C_4h^6–$I4_1/a$, number 88). Rare earth ions introduced into GdLF, YLF and LuLF replace the gadolinium (Gd), lutecium (Lu) and yttrium (Y) ions, respectively. The site symmetry of the Gd^{3+} and Lu^{3+} sites in GdLF and LuLF, respectively, is S_4, the same as for Y^{3+} ions in YLF. This means that while the overall symmetry of the GdLF, YLF and LuLF crystals is tetragonal, the symmetry at the site of the Gd^{3+}, Y^{3+} and Lu^{3+} ions in these crystals is S_4, so called because there exists a four-fold rotation–reflection axis. A four-fold rotation–reflection axis is one in which a rotation of $\pi/2$ followed by a reflection in the plane perpendicular to this axis produces an invariant configuration. This crystallographic detail plays an important role in determining the electric dipole–dipole transition selection rules in these laser crystals. The electric dipole (ED) selection rule table for S_4 site symmetry, applicable to $XLiF_4$ materials, is given in table 1. It is noted that the term 'forbidden' does not mean that the transition never occurs. It means that it is forbidden to first order. That is, it may occur in principle, but only with low probability in accordance with the probabilistic nature of quantum mechanics. The term 'forbidden' is inaccurate in a sense, but is historically embedded now in the nomenclature when discussing selection rules.

YLF and its isomorphs, LuLF and GdLF, are birefringent materials. The are also referred to as anisotropic crystals since they possess more than one axis that has a different refractive index. The crystallographic directions in GdLF, YLF and LuLF consist of two equivalent directions (the a-axes), and one unique direction (the c-axis). Crystals that exhibit this property are called uniaxial. GdLF and LuLF, like YLF, are uniaxial anisotropic crystals. Trivalent lanthanide ions replace, substitutionally, gadolinium (Gd^{3+}) ions in GdLF, yttrium (Y^{3+}) ions in YLF and lutecium (Lu^{3+}) ions in LuLF with only small changes in the lattice constants since the lanthanide ion Ho has nearly the same atomic radius. In fact, the effective ionic radii of Gd^{3+},

Table 1. Selection rules for electric dipole transitions in S_4 symmetry.

	Γ_1	Γ_2	Γ_3	Γ_4
Γ_1	Forbidden	π-pol.	σ-pol.	σ-pol.
Γ_2	π-pol.	Forbidden	σ-pol.	σ-pol.
Γ_3	σ-pol.	σ-pol.	Forbidden	π-pol.
Γ_4	σ-pol.	σ-pol.	π-pol.	Forbidden

Table 2. Lattice constants in GdLF, YLF and LuLF.

Material	a-axis (Å)	c-axis (Å)
GdLF	5.214	10.965
YLF	5.167	10.729
LuLF	5.124	10.540

Y^{3+} and Lu^{3+} are 105.3, 101.9 and 97.7 pm, respectively. The effective ionic radius of Ho^{3+} is 101.5 pm. These numbers are taken from Shannon [10] for a coordination number of 8. It is clear that Ho^{3+} ions are undersized for the Gd^{3+} in GdLF, almost the same size for the Y^{3+} ion in YLF, and oversized for the Lu^{3+} ion in LuLF.

The strength of the crystal field determines the spread in energy of the Stark levels of a manifold in a lanthanide ion in a crystal. The larger the crystal field, the larger the spread in Stark split levels. This observation makes sense in the context of measurements of the lattice constants for GdLF, YLF and LuLF [11, 12]. The relative strength of the crystal field for materials with similar structure can be assessed by comparison of the lattice constants, which are governed by the size of the host ions acting as dopant sites for the lanthanide ions. The lattice constants for GdLF, YLF and LuLF are given in table 2. From table 2, we see that the lattice constants for YLF are larger than LuLF, but smaller than GdLF. In simple terms this implies that YLF has a weaker crystal field than LuLF and a stronger crystal field than GdLF. It is, therefore, reasonable to expect the energy levels of lanthanide ions in GdLF to extend over a slightly smaller wavelength range than YLF and, similarly, for lanthanide ions in LuLF to extend over a slightly larger wavelength range than lanthanide ions in YLF. The crystal-field strength can be thought to 'stretch' the energy levels out. The higher the crystal field, the higher the 'stretching' is. The physical reasoning for this is that a tighter lattice exhibits larger crystal fields and larger crystal fields act to enhance the Stark effect. This Stark effect is a well known phenomenon. It is for this reason that garnets like $Y_3Al_5O_{12}$ (YAG) have a much larger Stark splitting for lanthanide dopant ions than fluorides such as GdLF, YLF and LuLF. For the same reason, GdLF has a slightly smaller Stark splitting than YLF, while LuLF has a slightly larger Stark splitting than YLF. The result is that when Ho^{3+} ions are substituted into GdLF and LuLF, they experience a weaker and stronger crystal field, respectively, than YLF. These small changes lead to a difference in the thermal populations of the upper and lower Ho laser levels, thus having an impact on the performance of the laser.

3. Experimental energy levels

The energy levels for Ho:YLF can be found in several publications in the literature [13–15]. There remains, however, a lack of information regarding the energy levels for Ho:GdLF and Ho:LuLF. The energy levels for the first ten manifolds in Ho:GdLF and Ho:LuLF are measured here. The energy levels in Ho:YLF have also been measured for completeness

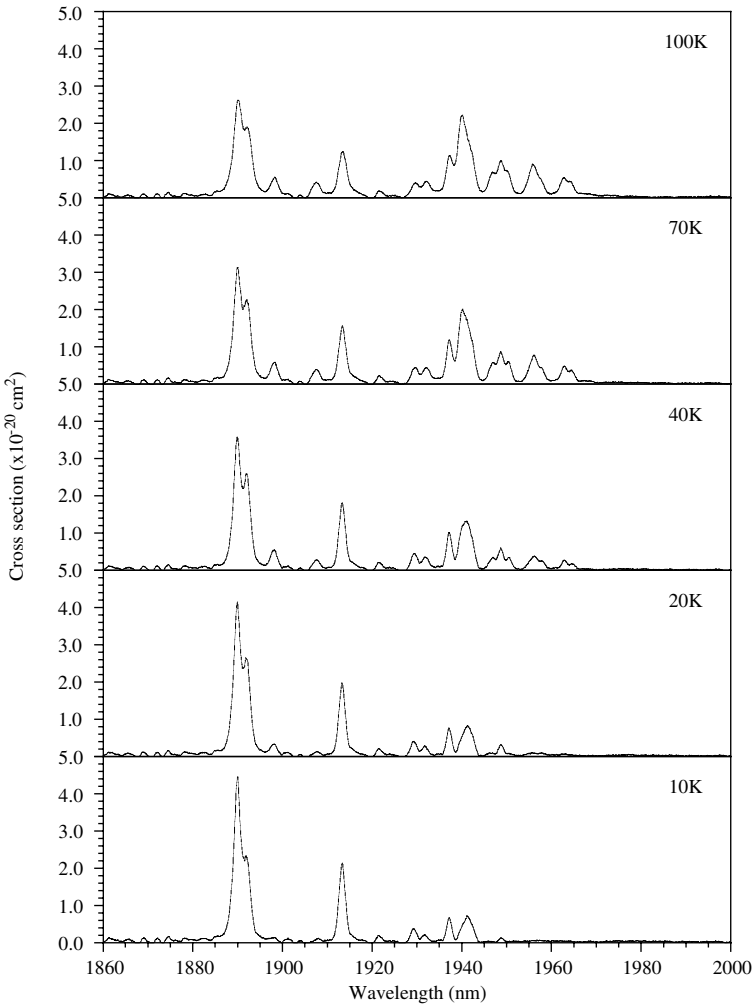

Figure 1. Temperature dependence of the π polarized Ho $^5I_7$ absorption in Ho:YLF from 10 to 100 K.

and for comparison with previously published results. The experimental energy levels of Ho:GdLF, Ho:YLF and Ho:LuLF were measured from polarized emission and absorption spectra at temperatures ranging from 10 to 300 K. Spectra at a number of temperatures in this range are necessary to determine the energy level placement of the various Stark levels. As a representative example, the temperature dependences of the absorption spectra of the Ho $^5I_7$ manifold for π and σ polarization are shown in figures 1 and 2. Figure 1 shows the π polarized absorption cross section from 10 to 100 K. Figure 2 shows the σ polarized absorption cross section from 10 to 100 K. It is clear from these figures that the spectral lines at the lower wavelength range decrease in absorption cross section with increasing temperature, while those in the upper wavelength range increase with increasing temperature. This is due to the Boltzmann statistics that governs the distribution of thermal population among the Stark levels inside a manifold. The thermal population or Boltzmann fraction inside a manifold is

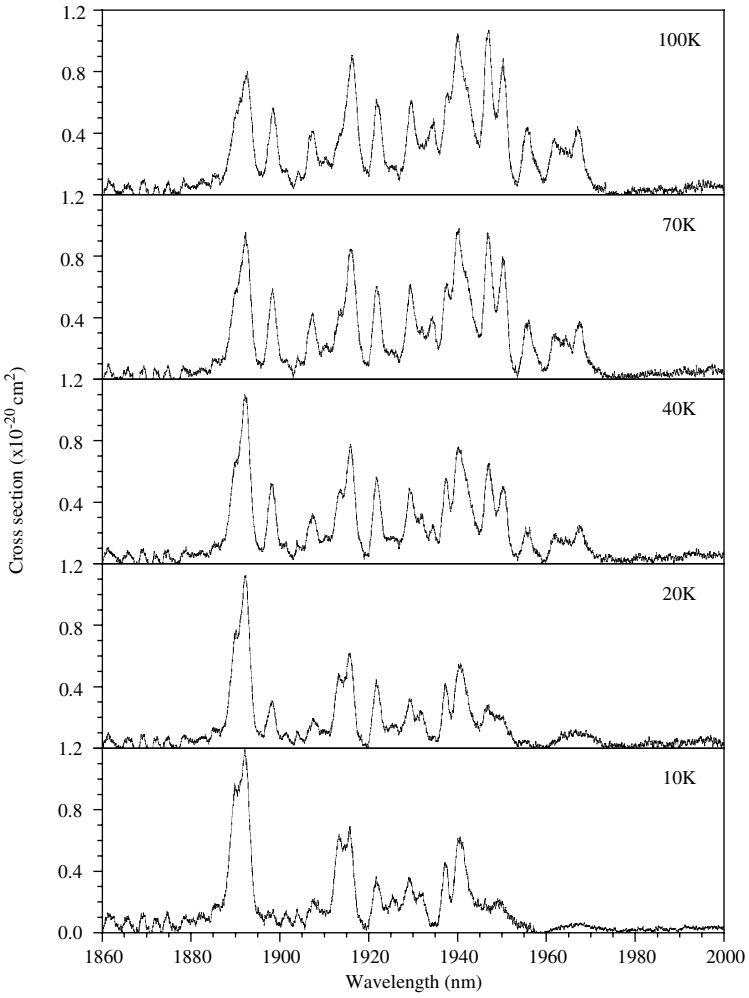

Figure 2. Temperature dependence of the σ polarized Ho $^5I_7$ absorption in Ho:YLF from 10 to 100 K.

given by

$$f_i = \frac{\exp(E_i/kT)}{\sum_j \exp(E_j/kT)} \tag{1}$$

where f_i is the fraction thermally excited in the ith Stark level within a given manifold. E_i is the energy in cm^{-1} of the ith Stark level within a given manifold. k is Boltzmann's constant and T is the temperature. The summation over j, known as the partition function, sums over all thermally populated Stark levels in the manifold. As the temperature is raised, Stark levels lying higher in energy in the ground state become more populated, while those lying lower in energy become less populated. This leads to the observed behaviour in figures 1 and 2. This also applies to the higher lying manifolds covered here. Of course, not all spectral lines either increase or decrease in intensity. Some spectral lines may initially increase in intensity with temperature as that particular Stark level becomes more thermally populated due to contributions from lower lying energy levels, and then decrease in intensity with even

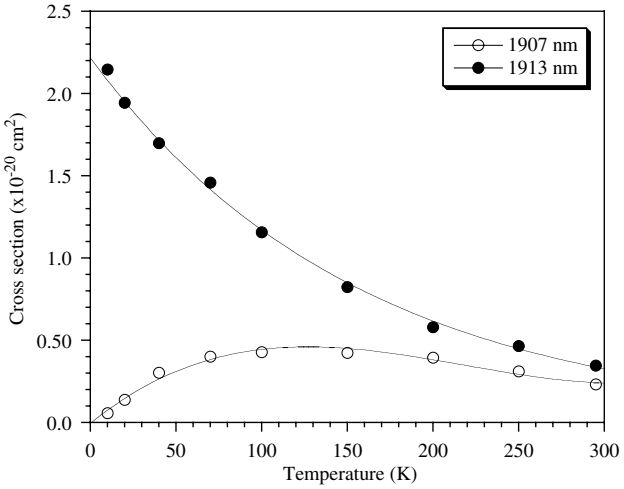

Figure 3. Cross section versus temperature for spectral lines at 1907 and 1914 nm in $^5I_8 \rightarrow {}^5I_7$ Ho:YLF π-pol. absorption.

higher temperature as the thermal population is distributed in higher lying energy levels. This is easily understood, but presents a very complicated situation to untangle the plethora of possibilities for assigning energy level values to each Stark level.

Obtaining the spectra over a wide wavelength range and at many different temperatures is certainly beneficial, but even when this is done there can remain some ambiguity on the assignment of levels. An analysis of the temperature dependence of the absorption cross section for individual lines can remove some ambiguities when considered in terms of Boltzmann statistics. This is best illustrated by an example. Figure 3 shows the absorption cross section dependence on temperature for two close lying lines in the $^5I_7$ manifold. The temperature dependence is different in behaviour for these two lines. The line at 1913 nm initially shows a rise with increasing temperature, but then declines steadily after 100 K. The line at 1907 nm always decreases with increasing temperature. The latter indicates a level that terminates at the lowest Stark level of the ground manifold, the $^5I_8$, in this case. The former terminates at some level above the zero level ground state. This behaviour of the absorption cross section is the same as the fractional population predicted by Boltzmann statistics and is very useful for assigning levels that have some ambiguity, and especially for finding levels that terminate to the lowest lying level of zero energy in the ground state.

Temperature dependent absorption spectra can aid in determining a great many energy levels of excited states, but temperature dependent emission spectra is crucial in determining the ground state energy levels. Some low temperature emission spectra are shown in figure 4. These manifolds in the visible wavelength region are particularly useful in determining some of the ground state energy levels. They have a low total angular momentum, J, and therefore fewer transitions, which is very useful in making assignments without the complication of an abundance of possibilities. The absorption spectra and Boltzmann statistics can be used initially to make some energy level assignments for the upper manifold, and then the emission spectra can be further analysed to determine the ground state levels. Once a set of ground state levels has been determined, it becomes much easier to fill in some of the more ambiguous assignments. This is a process that takes a great deal of patience and careful comparison of a great many spectra and their temperature dependence. Even in the most careful analysis of

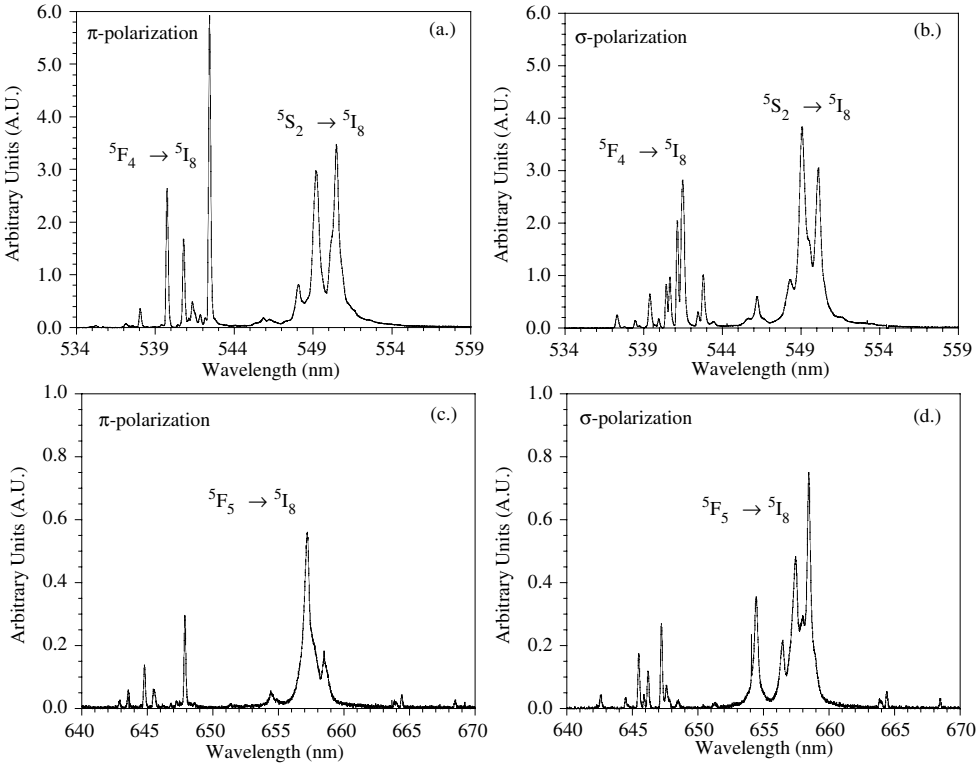

Figure 4. Emission spectra of $^5S_2 \rightarrow {}^5I_8$, $^5F_4 \rightarrow {}^5I_8$ and $^5F_5 \rightarrow {}^5I_8$ transitions in Ho:YLF at 10 K.

the large quantity of experimental data necessary for such measurements, it is not possible to determine all the energy levels experimentally. It is for this reason that some of the experimental energy levels do not appear in the tables that are presented later in this paper. To illustrate the diversity of the spectra even at very low temperatures approaching 8 K, figure 5 shows the absorption cross section for the six lowest manifolds in Ho:LuLF, excluding the Ho $^5I_4$ manifold, which exhibits no absorption. It should be mentioned that the observed spectra did not show any hypersensitive transitions in changing the host material, nor was there any clear evidence of multiple sites.

4. Crystal-field analysis

Because it is not possible in most cases to find all the energy levels experimentally, due to weak transitions and overlapping transitions, an iterative least squares fitting procedure between the experimental levels that can be measured and those generated from a suitable set of crystal-field parameters is employed. It is noted that not all energy levels could be directly measured for the reasons just stated. The crystal-field Hamiltonian can be written as

$$H_{\mathrm{CF}} = \sum_{k,m} B_{km}^{\dagger} \sum_{i} C_{km}(i) \tag{2}$$

where B_{km} are the crystal-field parameters satisfying

$$B_{km}^{\dagger} = (-1)^m B_{k,-m} \tag{3}$$

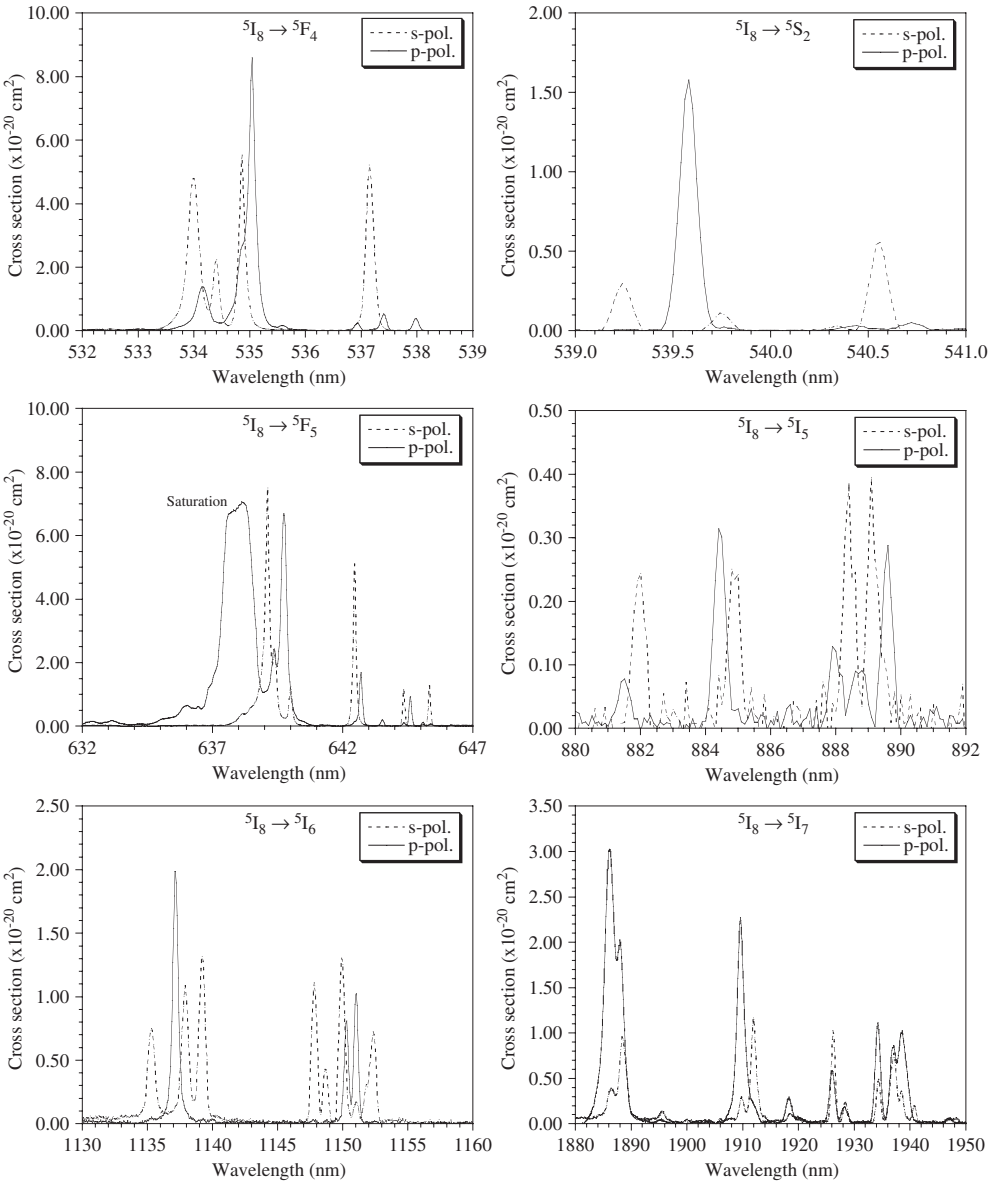

Figure 5. Absorption spectra of the σ and π polarized absorption in Ho:LuLF at 10 K.

and C_{km} are spherical tensors defined in terms of spherical harmonics, $Y_{km}(\theta_i, \phi_i)$, according to

$$C_{km}(i) = \left(\frac{4\pi}{2k+1}\right)^{1/2} Y_{km}(\theta_i, \phi_i). \tag{4}$$

In (2) the sums on k and m run over $k = 2, 4, 6$ and $m = 0, \pm 2, \ldots, \pm k$, and the sum on i runs over the number of electrons in the $4f^n$ configuration. In (4), θ_i and ϕ_i are the angular coordinates of the ith electron. The B_{km} used for the determination of energy levels are always even in k because the even parts of the expansion of the crystal-field potential contribute to

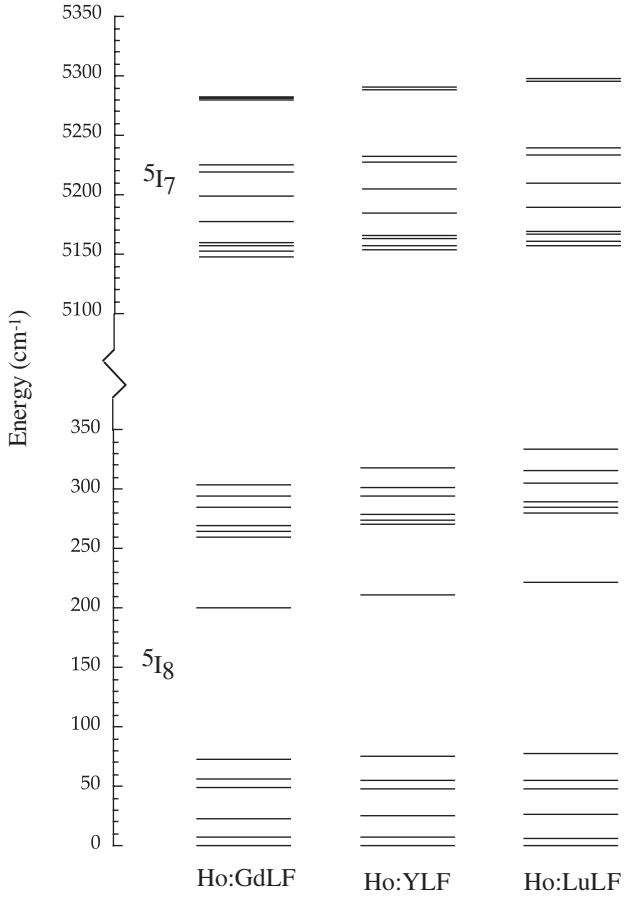

Figure 6. Theoretical energy levels of the two lowest manifolds in Ho:GdLF, Ho:YLF and Ho:LuLF.

the splitting and shifting of energy levels, while the odd parts are responsible for the mixing of opposite parity states from higher lying configurations into the $4f^n$ configuration. The later odd-order terms are important for the Judd–Ofelt theory, which is discussed in the next section. It is noted that $k = 0$ is always ignored because it represents a spherically symmetric crystal field that shifts all energy levels equally without affecting the energy level splitting. It is the crystal-field parameters, B_{km}, that describe the effects of the crystal field on the free-ion Hamiltonian. The free-ion Hamiltonian used in this analysis has the form

$$H_{\mathrm{FI}} = \sum_{k=0}^{3} e_k E^k + \alpha L(L+1) + \beta G(G_2) + \gamma G(G_7) + \zeta \sum_{i=1}^{N} (\vec{s}_i \cdot \vec{l}_i). \tag{5}$$

The first term in (5) represents the electron–electron intra-shell Coulomb interaction between 4f electrons. The second, third and fourth terms are two-body electron–electron configuration interaction terms representing interactions between electron configurations of the same parity. The fifth term is the spin–orbit coupling, representing the magnetic dipole–dipole interactions between the spin and angular magnetic moments of the 4f electrons. This is a seven parameter free-ion Hamiltonian. E^k ($k = 1, 2, 3$) are the Racah parameters corresponding to linear combinations of Slater radial integrals. α, β, and γ are parameters corresponding

Table 3. Even-order crystal-field parameters in Ho:GdLF, Ho:YLF and Ho:LuLF as determined from energy level fitting.

Material	B_{20}	B_{40}	B_{44}	B_{60}	B_{64}	iB_{64}
Ho:GdLF	380	−582	836	−53	627	113
Ho:YLF	389	−629	854	−33	661	127
Ho:LuLF	398	−666	870	−19	695	148

to linear combinations of radial factors and excitation energies of the 4f electrons to the electrons of the perturbing configuration. These parameters are sometimes referred to as 'Trees' parameters. ζ is the spin–orbit parameter, which is a radial integral. All of these parameters contain the radial dependence of the Hamiltonian. The angular dependence of the Hamiltonian is expressed in the operators e_k, L^2, $G(G_2)$, $G(R_7)$, and $\vec{s} \cdot \vec{l}$. These are, respectively, the angular spherical harmonic operators of the Coulomb potential, the angular momentum operator, the Casimir operator for Lie group G_2, the Casimir operator for Lie group R_7, and the spin–orbit operator. This separation of the free-ion Hamiltonian into radial parameters and angular operators is done because reliable radial wavefunctions cannot be generated. Instead, the radial parts of the Hamiltonian are treated as adjustable parameters. Even if reliable electrostatic and spin–orbit radial wavefunctions were known, the configuration interaction would still present a problem.

The theoretical calculations of the energy levels in Ho:LuLF were performed using software developed at the Harry Diamond Laboratories (HDL), now the Army Research Laboratories (ARL), in the 1970s. The principal personnel involved in the development of this software were Clyde Morrison, Richard Leavitt and Nick Karayanis. Representative papers covering applications using this software can be found in two papers by Morrison and Leavitt [16, 17]. Free-ion wavefunctions in a Russel–Saunders basis were calculated by diagonalizing the Hamiltonian given in (5). The free-ion parameters used were those given by Carnall, Fields and Rajnak for Ho in aqueous solution [18]. The Russel–Saunders (SLJ) wavefunctions were used as basis states to form a linear superposition of states for intermediate coupling ($[SL]J$), from which the reduced matrix elements of $U^{(2)}$, $U^{(4)}$, $U^{(6)}$ between all the intermediate-coupled wavefunctions for the $4f^{12}$ free-ion configuration of Ho were calculated. Ten manifolds were used in a truncated set of intermediate-coupled states to set up the crystal space for the S_4 crystal-field symmetry appropriate for GdLF, YLF and LuLF. The crystal-field Hamiltonian given in (2) is diagonalized together with an effective free-ion Hamiltonian of the form

$$H_{\mathrm{FI}} = \sum_{[SL]J} E_{[SL]J} |[SL]J\rangle\langle[SL]J| \tag{6}$$

where $E_{[SL]J}$ are the centroids of the energy manifolds. The free-ion values of the centroids are used as initial parameters.

The fitting procedure of experimental and theoretical energy levels consists of first fitting the centroids while keeping the crystal-field parameters constant. This adjusts the free-ion centroid positions of the manifolds to their approximate value for the ion in the presence of the crystal field of the host. The fit then proceeds by letting the crystal-field parameters vary in an iterative process until a least squares minimum is obtained between the calculated and measured energy levels. The initial value of the crystal-field parameters can be approximated theoretically [16], but we used the crystal-field parameters of Karayanis [13] for Ho:YLF as an initial guess in the energy level fitting.

Table 4. Experimental and theoretical energy levels in Ho:GdLF at 10 K.

Level	IR	Energy (theo.) (cm^{-1})	Energy (exp.) (cm^{-1})	Centroid (cm^{-1})	Free-ion mixture
1	$\Gamma_{3,4}$	−0.1	0.0		99.94 5I8 + 0.03 5I7 + 0.01 5F5
2	Γ_2	7.7	8.5		99.96 5I8 + 0.02 5I7 + 0.01 5F5
3	Γ_2	23.1	20.2		99.95 5I8 + 0.03 5I7 + 0.01 5F5
4	Γ_1	48.4	47.0		99.97 5I8 + 0.01 5I6 + 0.01 5I7
5	Γ_1	56.2	57.6		99.96 5I8 + 0.02 5I7 + 0.01 5I6
6	$\Gamma_{3,4}$	72.9	70.2	5I8	99.95 5I8 + 0.03 5I7 + 0.01 5F5
7	Γ_1	200.3	198.0	(164)	99.85 5I8 + 0.13 5I7 + 0.01 5G6
8	$\Gamma_{3,4}$	259.6	—		99.94 5I8 + 0.04 5I7 + 0.01 5I6
9	Γ_1	264.3	—		99.91 5I8 + 0.07 5I7 + 0.01 5I6
10	Γ_2	269.7	—		99.93 5I8 + 0.06 5I7
11	Γ_1	284.2	—		99.96 5I8 + 0.02 5I6 + 0.01 5I7
12	$\Gamma_{3,4}$	294.4	295.0		99.91 5I8 + 0.08 5I7 + 0.01 5F4
13	Γ_2	303.4	304.0		99.93 5I8 + 0.05 5I7 + 0.01 5F4
14	Γ_2	5 147.6	5 149.0		99.87 5I7 + 0.06 5I8 + 0.04 5I6
15	$\Gamma_{3,4}$	5 152.1	5 153.0		99.86 5I7 + 0.05 5I8 + 0.04 5I6
16	Γ_2	5 157.6	5 157.0		99.85 5I7 + 0.07 5I6 + 0.06 5I8
17	Γ_1	5 160.0	—		99.78 5I7 + 0.08 5I6 + 0.07 5I8
18	$\Gamma_{3,4}$	5 177.9	5 178.0	5I7	99.81 5I7 + 0.08 5I8 + 0.06 5I6
19	Γ_1	5 199.5	5 198.0	(5211)	99.82 5I7 + 0.15 5I8 + 0.01 5I6
20	$\Gamma_{3,4}$	5 219.7	5 219.0		99.82 5I7 + 0.11 5I6 + 0.04 5I8
21	Γ_2	5224.7	5 223.0		99.85 5I7 + 0.11 5I6 + 0.02 5I8
22	Γ_2	5 279.9	—		99.87 5I7 + 0.10 5I6 + 0.02 5I8
23	$\Gamma_{3,4}$	5 281.5	5 283.0		99.86 5I7 + 0.07 5I6 + 0.03 5I5
24	Γ_1	5 282.1	5 283.0		99.83 5I7 + 0.08 5I6 + 0.05 5I5
25	Γ_2	8 665.5	8 665.0		99.72 5I6 + 0.22 5I5 + 0.04 5I7
26	Γ_1	8 665.8	—		99.79 5I6 + 0.10 5I5 + 0.03 5F4
27	$\Gamma_{3,4}$	8 672.8	8 672.0		99.75 5I6 + 0.10 5I5 + 0.09 5I7
28	$\Gamma_{3,4}$	8 678.3	8 680.0		99.67 5I6 + 0.15 5I5 + 0.13 5I7
29	Γ_2	8 679.9	8 682.0	5I6	99.60 5I6 + 0.25 5I5 + 0.07 5I4
30	Γ_1	8 688.9	—	(8711)	99.76 5I6 + 0.16 5I7 + 0.03 5F5
31	Γ_2	8 692.3	8 692.0		99.69 5I6 + 0.13 5I7 + 0.08 5I4
32	Γ_1	8 762.5	8 762.0		99.67 5I6 + 0.23 5I5 + 0.08 5I4
33	$\Gamma_{3,4}$	8 775.6	8 773.0		99.77 5I6 + 0.10 5I5 + 0.07 5I7
34	Γ_2	8 787.6	8 785.0		99.88 5I6 + 0.10 5I7 + 0.01 5F3
35	Γ_1	112 35.8	11 237.0		99.24 5I5 + 0.59 5I4 + 0.12 5I6
36	$\Gamma_{3,4}$	11 236.1	—		99.87 5I5 + 0.05 5I7 + 0.02 5F3
37	$\Gamma_{3,4}$	11 238.5	—		99.62 5I5 + 0.17 5I4 + 0.10 5I6
38	Γ_2	11 243.3	11 243.0	5I5	99.62 5I5 + 0.25 5I6 + 0.06 5I4
39	Γ_1	11 245.8	11 250.0	(11 271)	99.53 5I5 + 0.31 5I6 + 0.11 5I4
40	Γ_1	11 297.3	11 295.0		98.99 5I5 + 0.95 5I4 + 0.02 5I6
41	$\Gamma_{3,4}$	11 322.6	11 321.0		99.69 5I5 + 0.14 5I6 + 0.13 5I4
42	Γ_2	113 28.4	11 327.0		99.62 5I5 + 0.27 5I6 + 0.05 5I4
43	Γ_1	13 185.1	13 186.0		99.77 5I4 + 0.09 5I5 + 0.08 5I6
44	$\Gamma_{3,4}$	13 263.2	13 263.0		99.52 5I4 + 0.31 5I5 + 0.05 5I6
45	Γ_2	13 318.4	13 319.0	5I4	99.82 5I4 + 0.08 5I6 + 0.03 5I5
46	Γ_1	13 330.6	13 330.0	(13 331)	98.99 5I4 + 0.97 5I5 + 0.02 5F1
47	Γ_2	13 342.7	13 342.0		99.77 5I4 + 0.08 5I6 + 0.07 5I5
48	$\Gamma_{3,4}$	13 401.5	13 403.0		99.38 5I4 + 0.58 5I5 + 0.01 5F5
49	Γ_1	13 518.5	13 517.0		99.94 5I4 + 0.03 5I6 + 0.02 5F4

Table 4. (Continued.)

Level	IR	Energy (theo.) (cm^{-1})	Energy (exp.) (cm^{-1})	Centroid (cm^{-1})	Free-ion mixture
50	Γ_2	15 487.2	15 487.0		99.88 5F5 + 0.02 5F4 + 0.02 5I5
51	$\Gamma_{3,4}$	15 492.7	15 492.0		99.89 5F5 + 0.03 5F4 + 0.02 5F3
52	Γ_1	15 509.6	15 512.0		99.88 5F5 + 0.04 5F3 + 0.04 5F4
53	Γ_1	15 551.8	15 557.0	5F5	99.77 5F5 + 0.12 5F4 + 0.03 5F2
54	$\Gamma_{3,4}$	15 618.4	15 615.0	(15 579)	99.84 5F5 + 0.05 5G6 + 0.03 5F4
55	Γ_2	15 630.0	15 625.0		99.79 5F5 + 0.08 5G6 + 0.04 5I6
56	Γ_1	15 636.0	15 632.0		99.84 5F5 + 0.05 5G6 + 0.03 5I7
57	$\Gamma_{3,4}$	15 653.3	15 659.0		99.93 5F5 + 0.02 5G6 + 0.02 5I6
58	Γ_2	18 489.2	18 484.0		92.52 5S2 + 7.29 5F4 + 0.11 5G6
59	Γ_1	18 494.0	18 488.0	5S2	90.00 5S2 + 9.83 5F4 + 0.06 5F5
60	$\Gamma_{3,4}$	18 516.8	18 520.0	(18 515)	98.94 5S2 + 0.89 5F4 + 0.07 5G6
61	Γ_2	18 521.4	18 528.0		99.44 5S2 + 0.32 5F4 + 0.19 5G6
62	Γ_2	18 601.6	18 604.0		92.33 5F4 + 7.25 5S2 + 0.18 5G6
63	Γ_1	18 603.6	18 606.0		92.55 5F4 + 7.14 5S2 + 0.12 5G6
64	$\Gamma_{3,4}$	18 615.5	18 612.0	5F4	99.66 5F4 + 0.14 5F3 + 0.06 5G6
65	Γ_1	18 677.7	18 679.0	(18 651)	99.41 5F4 + 0.22 5S2 + 0.19 5F3
66	$\Gamma_{3,4}$	18 679.3	18 685.0		98.95 5F4 + 0.87 5S2 + 0.08 5G6
67	Γ_2	18 699.6	18 695.0		99.41 5F4 + 0.33 5S2 + 0.17 5G6
68	Γ_1	18 706.5	18 704.0		97.27 5F4 + 2.50 5S2 + 0.12 5F2
69	$\Gamma_{3,4}$	20 643.9	20 643.0		99.56 5F3 + 0.16 5F1 + 0.07 5F4
70	Γ_1	20 669.0	20 670.0	5F3	99.52 5F3 + 0.20 5F4 + 0.16 3G5
71	Γ_2	20 711.1	20 710.0	(20 710)	99.25 5F3 + 0.38 5G6 + 0.32 5F2
72	Γ_2	20 760.2	20 761.0		98.52 5F3 + 0.72 5F2 + 0.68 5G6
73	$\Gamma_{3,4}$	20 766.7	20 767.0		99.43 5F3 + 0.21 5G6 + 0.11 5F2
74	Γ_2	21 103.6	21 104.0		98.92 5F2 + 0.67 5F3 + 0.18 5F4
75	Γ_1	21 112.2	21 111.0	5F2	99.57 5F2 + 0.20 5F4 + 0.07 3G5
76	$\Gamma_{3,4}$	21 148.3	21 149.0	(21 140)	98.95 5F2 + 0.49 5G6 + 0.17 5F3
77	Γ_2	21 202.0	21 202.0		99.25 5F2 + 0.30 5F3 + 0.18 5G6

The crystal-field parameters were varied to determine the best fit between experimental and theoretical energy levels. The crystal-field parameters determined from the energy level fitting in GdLF, YLF and LuLF are given in table 3. The experimental and theoretical energy levels for the first ten manifolds, the $^5I_8$ ground state through the $^5F_2$ excited state, for Ho:GdLF, Ho:YLF and Ho:LuLF are given in tables 4, 5 and 6, respectively. The second column in these tables is the irreducible representation (IR) of the Stark level. Stark levels with the IR $\Gamma_{3,4}$ are degenerate. The IR can be used to determine the selection rules for π and σ polarized transitions. The selection rules for electric dipole–dipole transitions in S_4 symmetry are shown in table 1. The energy level diagram for the Ho $^5I_7$ excited manifold and the Ho $^5I_8$ ground manifold of Ho:GdLF, Ho:YLF and Ho:LuLF is shown in figure 6 for comparison. The energy levels determined here for Ho:YLF are in excellent agreement with previous studies [13–15] adding confidence to the energy levels determined here for Ho:LuLF and Ho:GdLF.

5. Judd–Ofelt analysis

The Judd–Ofelt theory [19, 20] allows for the calculation of manifold to manifold transition probabilities, from which the radiative lifetimes and branching ratios of emission can be

Table 5. Experimental and theoretical energy levels in Ho:YLF at 10 K.

Level	IR	Energy (theo.) (cm^{-1})	Energy (exp.) (cm^{-1})	Centroid (cm^{-1})	Free-ion mixture
1	$\Gamma_{3,4}$	−0.1	0.1		99.94 5I8 + 0.03 5I7 + 0.01 5F5
2	Γ_2	6.8	7.0		99.95 5I8 + 0.02 5I7 + 0.01 5F5
3	Γ_2	24.6	23.0		99.94 5I8 + 0.03 5I7 + 0.01 5F5
4	Γ_1	47.8	48.0		99.96 5I8 + 0.01 5I6 + 0.01 5I7
5	Γ_1	55.2	57.0		99.95 5I8 + 0.03 5I7 + 0.01 5I6
6	$\Gamma_{3,4}$	74.7	72.0	5I8	99.95 5I8 + 0.03 5I7 + 0.01 5F5
7	Γ_1	211.3	213.0	(171)	99.84 5I8 + 0.15 5I7 + 0.01 5G6
8	$\Gamma_{3,4}$	269.8	—		99.93 5I8 + 0.05 5I7 + 0.01 5I6
9	Γ_1	273.9	—		99.90 5I8 + 0.08 5I7 + 0.01 5I6
10	Γ_2	279.2	—		99.92 5I8 + 0.07 5I7
11	Γ_1	294.2	—		99.96 5I8 + 0.03 5I6 + 0.01 5I7
12	$\Gamma_{3,4}$	301.3	306.0		99.90 5I8 + 0.09 5I7 + 0.01 5F4
13	Γ_2	317.9	314.0		99.92 5I8 + 0.06 5I7 + 0.01 5F4
14	Γ_2	5 153.3	5 152.0		99.85 5I7 + 0.07 5I8 + 0.04 5I6
15	$\Gamma_{3,4}$	5 157.2	5 156.0		99.85 5I7 + 0.06 5I8 + 0.04 5I6
16	Γ_2	5 163.3	5 163.0		99.84 5I7 + 0.07 5I6 + 0.07 5I8
17	Γ_1	5 165.3	—		99.76 5I7 + 0.09 5I6 + 0.08 5I8
18	$\Gamma_{3,4}$	5 184.5	5 185.0	5I7	99.80 5I7 + 0.08 5I8 + 0.07 5I6
19	Γ_2	5 205.3	5 205.0	(5218)	99.81 5I7 + 0.16 5I8 + 0.01 5I6
20	$\Gamma_{3,4}$	5227.3	5 228.0		99.80 5I7 + 0.13 5I6 + 0.04 5I8
21	Γ_2	5 232.7	5 232.0		99.83 5I7 + 0.12 5I6 + 0.02 5I8
22	Γ_2	5 288.4	—		99.85 5I7 + 0.11 5I6 + 0.02 5I8
23	$\Gamma_{3,4}$	5 290.3	5 291.0		99.85 5I7 + 0.09 5I6 + 0.04 5I5
24	Γ_1	5 291.1	5 293.0		99.81 5I7 + 0.09 5I6 + 0.06 5I5
25	Γ_2	8 669.7	—		99.69 5I6 + 0.24 5I5 + 0.04 5I7
26	Γ_1	8 670.1	8 669.0		99.78 5I6 + 0.10 5I5 + 0.04 5I8
27	$\Gamma_{3,4}$	8 677.3	8 678.0		99.73 5I6 + 0.11 5I5 + 0.10 5I7
28	$\Gamma_{3,4}$	8 682.3	8 684.0		99.64 5I6 + 0.16 5I5 + 0.14 5I7
29	Γ_2	8 685.6	8 686.0	5I6	99.56 5I6 + 0.28 5I5 + 0.08 5I4
30	Γ_1	8 693.5	8 695.0	(8717)	99.74 5I6 + 0.18 5I7 + 0.03 5F5
31	Γ_2	8 699.5	8 700.0		99.66 5I6 + 0.14 5I7 + 0.09 5I4
32	Γ_1	8 768.8	8 768.0		99.63 5I6 + 0.25 5I5 + 0.08 5I4
33	$\Gamma_{3,4}$	8 783.4	8 782.0		99.75 5I6 + 0.11 5I5 + 0.08 5I7
34	Γ_2	8 796.5	8 795.0		99.87 5I6 + 0.11 5I7 + 0.01 5F3
35	Γ_1	11 242.2	11 242.0		99.86 5I5 + 0.06 5I7 + 0.02 5F3
36	$\Gamma_{3,4}$	11 242.8	—		99.17 5I5 + 0.65 5I4 + 0.13 5I6
37	$\Gamma_{3,4}$	11 245.4	11 248.0		99.59 5I5 + 0.18 5I4 + 0.10 5I6
38	Γ_2	11 250.6	11 250.0	5I5	99.59 5I5 + 0.27 5I6 + 0.07 5I4
39	Γ_1	11 252.1	11 256.0	(11 279)	99.49 5I5 + 0.34 5I6 + 0.12 5I4
40	Γ_1	11 304.3	11 302.0		98.88 5I5 + 1.04 5I4 + 0.02 5I6
41	$\Gamma_{3,4}$	11 332.0	11 330.0		99.64 5I5 + 0.16 5I4 + 0.15 5I6
42	Γ_2	11 338.3	11 337.0		99.57 5I5 + 0.30 5I6 + 0.07 5I4
43	Γ_1	13 188.3	13 187.0		99.75 5I4 + 0.10 5I5 + 0.09 5I6
44	$\Gamma_{3,4}$	13 269.3	13 269.0		99.49 5I4 + 0.33 5I5 + 0.05 5I6
45	Γ_2	13 321.1	13 320.0	5I4	99.81 5I4 + 0.09 5I6 + 0.04 5I5
46	Γ_1	13 340.8	13 340.0	(13 339)	98.89 5I4 + 1.07 5I5 + 0.03 5F1
47	Γ_2	13 349.1	13 350.0		99.74 5I4 + 0.09 5I6 + 0.08 5I5
48	$\Gamma_{3,4}$	13 412.5	13 414.0		99.31 5I4 + 0.65 5I5 + 0.01 5F5
49	Γ_1	13 536.8	13 538.0		99.93 5I4 + 0.03 5I6 + 0.02 5F4

Table 5. (Continued.)

Level	IR	Energy (theo.) (cm^{-1})	Energy (exp.) (cm^{-1})	Centroid (cm^{-1})	Free-ion mixture
50	Γ_2	15 488.8	15 489.0		99.87 5F5 + 0.02 5F4 + 0.02 5I5
51	$\Gamma_{3,4}$	15 493.9	15 495.0		99.88 5F5 + 0.03 5F4 + 0.02 5F3
52	Γ_1	15 511.2	15 512.0		99.87 5F5 + 0.04 5F4 + 0.04 5F3
53	Γ_1	15 552.8	15 558.0	5F5	99.75 5F5 + 0.13 5F4 + 0.04 5F2
54	$\Gamma_{3,4}$	15 624.3	15 622.0	(15 582)	99.82 5F5 + 0.06 5G6 + 0.03 5F4
55	Γ_2	15 635.4	15 631.0		99.78 5F5 + 0.09 5G6 + 0.04 5I6
56	Γ_1	15 641.8	15 638.0		99.83 5F5 + 0.05 5G6 + 0.04 5I7
57	$\Gamma_{3,4}$	15 660.8	15 664.0		99.92 5F5 + 0.02 5I6 + 0.02 5G6
58	Γ_2	18 491.9	18 487.0		91.37 5S2 + 8.42 5F4 + 0.12 5G6
59	Γ_1	18 496.5	18 490.0	5S2	88.88 5S2 + 10.93 5F4 + 0.07 5F5
60	$\Gamma_{3,4}$	18 521.4	18 523.0	(18 519)	98.93 5S2 + 0.88 5F4 + 0.08 5G6
61	Γ_2	18 525.8	18 534.0		99.43 5S2 + 0.31 5F4 + 0.20 5G6
62	Γ_2	18 602.0	18 605.0		91.16 5F4 + 8.38 5S2 + 0.20 5G6
63	Γ_1	18 604.9	18 608.0		91.39 5F4 + 8.27 5S2 + 0.14 5G6
64	$\Gamma_{3,4}$	18 617.2	18 615.0	5F4	99.63 5F4 + 0.15 5F3 + 0.06 5G6
65	Γ_1	18 680.6	18 680.0	(18 654)	99.33 5F4 + 0.26 5S2 + 0.21 5F3
66	$\Gamma_{3,4}$	18 684.1	18 686.0		98.96 5F4 + 0.86 5S2 + 0.09 5G6
67	Γ_2	18 703.7	18 701.0		99.41 5F4 + 0.32 5S2 + 0.18 5G6
68	Γ_1	18 711.9	18 711.0		97.34 5F4 + 2.42 5S2 + 0.12 5F2
69	$\Gamma_{3,4}$	20 642.6	20 642.0		99.52 5F3 + 0.18 5F1 + 0.08 5F4
70	Γ_1	20 666.5	20 666.0	5F3	99.48 5F3 + 0.22 5F4 + 0.17 3G5
71	Γ_2	20 714.0	20 713.0	(20 710)	99.22 5F3 + 0.41 5G6 + 0.30 5F2
72	Γ_2	20 762.2	20 763.0		98.50 5F3 + 0.76 5G6 + 0.67 5F2
73	$\Gamma_{3,4}$	20 768.8	20 770.0		99.40 5F3 + 0.23 5G6 + 0.11 5F2
74	Γ_2	21 127.7	21 128.0		98.94 5F2 + 0.61 5F3 + 0.19 5F4
75	Γ_1	21 135.2	21 135.0	5F2	99.53 5F2 + 0.21 5F4 + 0.08 3K8
76	$\Gamma_{3,4}$	21 173.7	21 174.0	(21 167)	98.84 5F2 + 0.56 5G6 + 0.17 3G5
77	Γ_2	21 227.4	21 227.0		99.15 5F2 + 0.28 5F3 + 0.21 5G6

determined. A Judd–Ofelt analysis relies on accurate absorption measurements, specifically the integrated absorption cross section over the wavelength range of a number of manifolds. From the integrated absorption cross section, the so-called line strength, S_m, can be found:

$$S_m = \frac{3hc(2J'+1)}{8\pi^3 e^2 \bar{\lambda}} n \left(\frac{3}{n^2+2}\right)^2 \int \sigma(\lambda)\,\mathrm{d}\lambda \tag{7}$$

where J' is the total angular momentum of the initial ground manifold, found from the $^{2S+1}L_J$ designation. $\sigma(\lambda)$ is the emission cross section as a function of wavelength. The mean wavelength, $\bar{\lambda}$, can be found from the first moment of the absorption cross section data:

$$\bar{\lambda} = \frac{\sum \sigma(\lambda)}{\sum \lambda\sigma(\lambda)}. \tag{8}$$

The other symbols have their usual meaning. The utility of the Judd–Ofelt theory is that it provides a theoretical expression for the line strength, given by

$$S_{\mathrm{ED}}(aJ; bJ') = \sum_{\lambda=2,4,6} \Omega_\lambda |\langle f^n[SL]J||U^{(\lambda)}||f^n[S'L']J'\rangle|^2 \tag{9}$$

where Ω_λ are the Judd–Ofelt parameters. The terms in brackets are doubly reduced matrix elements for intermediate coupling. Intermediate coupling refers to a situation where the

Table 6. Experimental and theoretical energy levels in Ho:LuLF at 10 K.

Level	IR	Energy (theo.) (cm^{-1})	Energy (exp.) (cm^{-1})	Centroid (cm^{-1})	Free-ion mixture
1	$\Gamma_{3,4}$	−0.2	0.0		99.93 5I8 + 0.04 5I7 + 0.01 5F5
2	Γ_2	6.1	7.5		99.95 5I8 + 0.03 5I7 + 0.01 5F5
3	Γ_2	26.9	27.6		99.94 5I8 + 0.03 5I7 + 0.02 5F5
4	Γ_1	48.2	47.2		99.96 5I8 + 0.02 5I6 + 0.01 5I7
5	Γ_1	55.1	57.8		99.95 5I8 + 0.03 5I7 + 0.01 5I6
6	$\Gamma_{3,4}$	77.8	76.2	5I8	99.94 5I8 + 0.03 5I7 + 0.01 5F5
7	Γ_1	222.1	222.0	(178)	99.82 5I8 + 0.16 5I7 + 0.01 5G6
8	$\Gamma_{3,4}$	279.7	—		99.92 5I8 + 0.05 5I7 + 0.02 5I6
9	Γ_1	284.9	—		99.89 5I8 + 0.08 5I7 + 0.01 5I6
10	Γ_2	288.9	—		99.91 5I8 + 0.08 5I7
11	Γ_1	305.1	—		99.95 5I8 + 0.03 5I6 + 0.01 5I7
12	$\Gamma_{3,4}$	315.6	315.0		99.89 5I8 + 0.10 5I7 + 0.01 5F4
13	Γ_2	333.7	332.0		99.91 5I8 + 0.07 5I7 + 0.01 5F4
14	Γ_2	5 154.5	5 154.4		99.84 5I7 + 0.08 5I8 + 0.05 5I6
15	$\Gamma_{3,4}$	5 157.1	5 157.3		99.84 5I7 + 0.07 5I8 + 0.04 5I6
16	Γ_2	5 167.4	5 167.0		99.82 5I7 + 0.08 5I6 + 0.07 5I8
17	Γ_1	5 169.5	5 168.6		99.74 5I7 + 0.09 5I6 + 0.09 5I8
18	$\Gamma_{3,4}$	5 189.4	5 190.6	5I7	99.78 5I7 + 0.09 5I8 + 0.07 5I6
19	Γ_1	5 210.1	5 211.7	(5224)	99.79 5I7 + 0.18 5I8 + 0.01 5I6
20	$\Gamma_{3,4}$	5 233.4	5 229.6		99.78 5I7 + 0.15 5I6 + 0.04 5I8
21	Γ_2	5 239.1	5 235.3		99.82 5I7 + 0.14 5I6 + 0.02 5I8
22	Γ_2	5 295.2	5 295.0		99.84 5I7 + 0.12 5I6 + 0.02 5I8
23	$\Gamma_{3,4}$	5 297.3	5 299.1		99.83 5I7 + 0.10 5I6 + 0.04 5I5
24	Γ_1	5 298.2	5 301.6		99.79 5I7 + 0.10 5I6 + 0.06 5I5
25	Γ_2	8 675.0	—		99.66 5I6 + 0.26 5I5 + 0.04 5I7
26	Γ_1	8 676.0	8 674.3		99.76 5I6 + 0.11 5I5 + 0.04 5I8
27	$\Gamma_{3,4}$	8 683.2	8 684.5		99.70 5I6 + 0.12 5I5 + 0.11 5I7
28	$\Gamma_{3,4}$	8 688.3	8 692.8		99.61 5I6 + 0.18 5I5 + 0.15 5I7
29	Γ_2	8 692.2	8 690.2	5I6	99.51 5I6 + 0.31 5I5 + 0.08 5I4
30	Γ_1	8 699.9	8 702.2	(8724)	99.72 5I6 + 0.19 5I7 + 0.04 5F5
31	Γ_2	8 707.8	8 708.6		99.63 5I6 + 0.16 5I7 + 0.09 5I4
32	Γ_1	8 776.3	8 774.6		99.59 5I6 + 0.28 5I5 + 0.09 5I4
33	$\Gamma_{3,4}$	8 792.4	8 790.7		99.72 5I6 + 0.12 5I5 + 0.08 5I7
34	Γ_2	8 806.7	8 804.8		99.85 5I6 + 0.12 5I7 + 0.01 5F3
35	Γ_1	11 244.7	—		99.84 5I5 + 0.07 5I7 + 0.03 5F3
36	$\Gamma_{3,4}$	11 245.3	11 244.3		99.09 5I5 + 0.71 5I4 + 0.15 5I6
37	$\Gamma_{3,4}$	11 248.3	11 248.1		99.56 5I5 + 0.19 5I4 + 0.10 5I6
38	Γ_2	11 254.0	11 253.0	5I5	99.54 5I5 + 0.30 5I6 + 0.07 5I4
39	Γ_1	11 254.6	11 259.5	(11 283)	99.45 5I5 + 0.37 5I6 + 0.13 5I4
40	Γ_1	11 307.0	11 304.0		98.77 5I5 + 1.15 5I4 + 0.02 5I7
41	$\Gamma_{3,4}$	11 337.2	11 338.0		99.60 5I5 + 0.18 5I4 + 0.17 5I6
42	Γ_2	11 343.9	11 343.5		99.52 5I5 + 0.32 5I6 + 0.08 5I4
43	Γ_1	13 187.1	13 188.0		99.73 5I4 + 0.10 5I5 + 0.10 5I6
44	$\Gamma_{3,4}$	13 272.0	13 267.5		99.45 5I4 + 0.35 5I5 + 0.06 5I6
45	Γ_2	13 320.0	13 320.5	5I4	99.79 5I4 + 0.10 5I6 + 0.04 5I5
46	Γ_1	13 347.1	13 348.0	(13 343)	98.78 5I4 + 1.18 5I5 + 0.03 5F1
47	Γ_2	13 353.9	13 353.5		99.71 5I4 + 0.10 5I6 + 0.10 5I5
48	$\Gamma_{3,4}$	13 419.4	13 416.0		99.23 5I4 + 0.73 5I5 + 0.01 5F5
49	Γ_1	13 550.7	13 556.5		99.93 5I4 + 0.03 5I6 + 0.02 5F4

Table 6. (Continued.)

Level	IR	Energy (theo.) (cm^{-1})	Energy (exp.) (cm^{-1})	Centroid (cm^{-1})	Free-ion mixture
50	Γ_2	15 493.3	15 491.4		99.85 5F5 + 0.03 5F4 + 0.02 5I5
51	$\Gamma_{3,4}$	15 498.1	15 497.2		99.87 5F5 + 0.03 5F4 + 0.03 5F3
52	Γ_1	15 515.9	15 515.1		99.86 5F5 + 0.05 5F4 + 0.05 5F3
53	Γ_1	15 557.1	15 560.6	5F5	99.73 5F5 + 0.14 5F4 + 0.04 5F2
54	$\Gamma_{3,4}$	15 632.5	15 635.1	(15 589)	99.81 5F5 + 0.06 5G6 + 0.03 5F4
55	Γ_2	15 643.2	15 642.0		99.76 5F5 + 0.09 5G6 + 0.04 5I6
56	Γ_1	15 649.9	15 648.0		99.82 5F5 + 0.05 5G6 + 0.04 5I7
57	$\Gamma_{3,4}$	15 670.3	15 671.0		99.92 5F5 + 0.02 5I6 + 0.02 5I7
58	Γ_2	18 491.5	18 488.5		91.07 5S2 + 8.71 5F4 + 0.12 5G6
59	Γ_1	18 496.2	18 498.3	5S2	88.69 5S2 + 11.11 5F4 + 0.07 5F5
60	$\Gamma_{3,4}$	18 522.4	18 521.8	(18 520)	98.98 5S2 + 0.82 5F4 + 0.09 5G6
61	Γ_2	18 526.4	18 527.6		99.43 5S2 + 0.29 5F4 + 0.21 5G6
62	Γ_2	18 604.0	18 602.7		90.84 5F4 + 8.66 5S2 + 0.21 5G6
63	Γ_1	18 607.2	18 611.2		91.01 5F4 + 8.62 5S2 + 0.15 5G6
64	$\Gamma_{3,4}$	18 620.9	18 619.3	5F4	99.60 5F4 + 0.17 5F3 + 0.06 5G6
65	Γ_1	18 685.7	18 684.9	(18 659)	99.24 5F4 + 0.32 5S2 + 0.22 5F3
66	$\Gamma_{3,4}$	18 690.3	18 691.0		99.01 5F4 + 0.79 5S2 + 0.09 5G6
67	Γ_2	18 710.0	18 707.1		99.41 5F4 + 0.31 5S2 + 0.19 5G6
68	Γ_1	18 719.6	18 721.8		97.55 5F4 + 2.21 5S2 + 0.12 5F2
69	$\Gamma_{3,4}$	20 644.0	20 643.9		99.49 5F3 + 0.19 5F1 + 0.10 5F4
70	Γ_1	20 667.3	20 668.8	5F3	99.43 5F3 + 0.24 5F4 + 0.18 3G5
71	Γ_2	20 719.0	20 719.9	(20 713)	99.17 5F3 + 0.45 5G6 + 0.31 5F2
72	Γ_2	20 766.1	20 761.9		98.40 5F3 + 0.83 5G6 + 0.68 5F2
73	$\Gamma_{3,4}$	20 773.6	20 775.4		99.36 5F3 + 0.26 5G6 + 0.11 5F2
74	Γ_2	21 134.9	21 137.2		98.89 5F2 + 0.62 5F3 + 0.21 5F4
75	Γ_1	21 141.4	21 142.0	5F2	99.50 5F2 + 0.22 5F4 + 0.09 3K8
76	$\Gamma_{3,4}$	21 181.5	21 180.0	(21 174)	98.73 5F2 + 0.62 5G6 + 0.18 3G5
77	Γ_2	21 235.7	21 234.3		99.04 5F2 + 0.29 5F3 + 0.25 3K8

Table 7. Measured and calculated values for the linestrength in Ho^{3+} GdLF.

Transition (from $^5I_8$)	$\lvert\langle U^{(2)}\rangle\rvert^2$	$\lvert\langle U^{(4)}\rangle\rvert^2$	$\lvert\langle U^{(6)}\rangle\rvert^2$	$\bar{\lambda}$ (nm)	Linestrength (10^{-20} cm^2)	
					Measured	Calculated
$^3K_6 + {}^3F_4$	0.0026	0.1263	0.0073	333	0.3407	0.3110
$^3L_9 + {}^5G_3$	0.0185	0.0052	0.1169	345	0.3790	0.4049
$^3D_2 + {}^3H_6 + {}^5G_5$	0.2155	0.1969	0.1679	361	1.3774	1.1038
$^3K_7 + {}^5G_4$	0.0058	0.0361	0.0697	385	0.3499	0.2450
$^3G_5$	0.0000	0.5338	0.0002	417	1.1993	1.2335
$^5F_1 + {}^5G_6$	1.5201	0.8410	0.1411	450	4.1774	4.2139
$^3K_8$	0.0208	0.0334	0.1535	467	0.2677	0.4433
$^3F_2$	0.0000	0.0000	0.2041	473	0.4456	0.4512
$^3F_3$	0.0000	0.0000	0.3464	485	0.8106	0.7659
$^5F_4 + {}^5S_2$	0.0000	0.2392	0.9339	539	2.5898	2.6173
$^5F_5$	0.0000	0.4250	0.5687	645	2.2411	2.2391
$^5I_5$	0.0000	0.0100	0.0936	897	0.1571	0.2300

mutual repulsion interaction between 4f electrons is of the same order of magnitude as the spin–orbit coupling. This effect can be incorporated by expanding the wavefunctions of the 4f states

Table 8. Calculated branching ratios and lifetimes in Ho^{3+} GdLF.

Transition	$\bar{\lambda}$ (nm)	S_{ED} (10^{-20} cm^2)	A_{ED} (s^{-1})	A_{MD} (s^{-1})	β	τ_r (ms)	τ_m (ms)
$^5F_2 \rightarrow {}^5F_3$	23 256	0.067	0.00		0.0000		
$^5F_2 \rightarrow {}^5F_4$	4 018	0.267	1.52		0.0004		
$^5F_2 \rightarrow {}^5S_2$	3 810	0.010	0.07		0.0000		
$^5F_2 \rightarrow {}^5F_4$	1 798	0.336	22.34		0.0063		
$^5F_2 \rightarrow {}^5I_4$	1 281	0.174	32.30		0.0091		
$^5F_2 \rightarrow {}^5I_5$	1 013	0.530	198.80		0.0558		
$^5F_2 \rightarrow {}^5I_6$	805	0.778	585.15		0.1641		
$^5F_2 \rightarrow {}^5I_7$	628	0.670	1066.96		0.2993		
$^5F_2 \rightarrow {}^5I_8$	477	0.451	1657.65		0.4650	0.281	
$^5F_3 \rightarrow {}^5F_4$	4 857	0.408	0.91		0.0002		
$^5F_3 \rightarrow {}^5S_2$	4 556	0.008	0.02		0.0000		
$^5F_3 \rightarrow {}^5F_5$	1 949	1.754	65.28		0.0178		
$^5F_3 \rightarrow {}^5I_4$	1 355	1.100	122.67		0.0335		
$^5F_3 \rightarrow {}^5I_5$	1 059	0.541	126.65		0.0346		
$^5F_3 \rightarrow {}^5I_6$	833	0.687	332.13		0.0908		
$^5F_3 \rightarrow {}^5I_7$	645	1.073	1123.38		0.3071		
$^5F_3 \rightarrow {}^5I_8$	487	0.766	1886.68		0.5158	0.273	
$^5F_4 \rightarrow {}^5S_2$	73 529	0.044	0.00		0.0000		
$^5F_4 \rightarrow {}^5F_5$	3 255	0.481	2.92	2.62	0.0008		
$^5F_4 \rightarrow {}^5I_4$	1 880	0.626	20.22		0.0057		
$^5F_4 \rightarrow {}^5I_5$	1 355	1.335	115.82		0.0324		
$^5F_4 \rightarrow {}^5I_6$	1 006	0.973	207.14		0.0580		
$^5F_4 \rightarrow {}^5I_7$	744	0.509	280.96		0.0786		
$^5F_4 \rightarrow {}^5I_8$	541	2.120	2946.29		0.8245	0.280	
$^5S_2 \rightarrow {}^5F_5$	3 406	0.033	0.32		0.0001		
$^5S_2 \rightarrow {}^5I_4$	1 929	0.684	36.76		0.0161		
$^5S_2 \rightarrow {}^5I_5$	1 381	0.245	36.13		0.0158		
$^5S_2 \rightarrow {}^5I_6$	1 020	0.388	142.78		0.0626		
$^5S_2 \rightarrow {}^5I_7$	752	0.906	836.64		0.3669		
$^5S_2 \rightarrow {}^5I_8$	545	0.502	1227.67		0.5384	0.439	
$^5F_5 \rightarrow {}^5I_4$	4 448	0.023	0.04		0.0000		
$^5F_5 \rightarrow {}^5I_5$	2 321	0.436	6.08		0.0032		
$^5F_5 \rightarrow {}^5I_6$	1 456	1.398	79.86		0.0420		
$^5F_5 \rightarrow {}^5I_7$	965	1.744	345.10		0.1814		
$^5F_5 \rightarrow {}^5I_8$	649	2.245	1471.64		0.7734	0.526	
$^5I_4 \rightarrow {}^5I_5$	4 854	2.338	4.06	1.49	0.0473		
$^5I_4 \rightarrow {}^5I_6$	2 164	1.536	32.35		0.3767		
$^5I_4 \rightarrow {}^5I_7$	1 232	0.354	41.00		0.4774		
$^5I_4 \rightarrow {}^5I_8$	760	0.017	8.47		0.0986	11.64	
$^5I_5 \rightarrow {}^5I_6$	3 906	1.717	4.85	3.85	0.0347		
$^5I_5 \rightarrow {}^5I_7$	1 650	2.021	79.13		0.5654		
$^5I_5 \rightarrow {}^5I_8$	900	0.230	55.97		0.3999	6.95	
$^5I_6 \rightarrow {}^5I_7$	2 857	2.408	15.09	8.77	0.0901		
$^5I_6 \rightarrow {}^5I_8$	1 170	1.629	152.30		0.9099	5.68	
$^5I_7 \rightarrow {}^5I_8$	1 981	3.707	61.24	15.41	1.0000	13.04	14.3

in a linear combination of Russel–Saunders, or LS coupled states. The coupling coefficients are found by diagonalizing the combined electrostatic, spin orbit and configuration interaction energy matrices to obtain the full intermediate-coupled wavefunctions, $|f^n[SL]\rangle$. A substantial

Table 9. Measured and calculated values for the linestrength in Ho^{3+} YLF.

Transition (from $^5I_8$)	$\|\langle U^{(2)}\rangle\|^2$	$\|\langle U^{(4)}\rangle\|^2$	$\|\langle U^{(6)}\rangle\|^2$	$\bar{\lambda}$ (nm)	Linestrength (10^{-20} cm^2)	
					Measured	Calculated
$^3K_6 + {}^3F_4$	0.0026	0.1263	0.0073	333	0.3095	0.2989
$^3L_9 + {}^5G_3$	0.0185	0.0052	0.1169	345	0.3639	0.3800
$^3D_2 + {}^3H_6 + {}^5G_5$	0.2155	0.1969	0.1679	361	1.3103	1.0373
$^3K_7 + {}^5G_4$	0.0058	0.0361	0.0697	385	0.3252	0.2319
$^3G_5$	0.0000	0.5338	0.0002	417	1.1614	1.1878
$^5F_1 + {}^5G_6$	1.5201	0.8410	0.1411	450	3.8926	3.9291
$^3K_8$	0.0208	0.0334	0.1535	467	0.2441	0.4175
$^3F_2$	0.0000	0.0000	0.2041	473	0.3918	0.4243
$^3F_3$	0.0000	0.0000	0.3464	485	0.7163	0.7202
$^5F_4 + {}^5S_2$	0.0000	0.2392	0.9339	538	2.4802	2.4737
$^5F_5$	0.0000	0.4250	0.5687	644	2.1068	2.1277
$^5I_5$	0.0000	0.0100	0.0936	899	0.1722	0.2168

portion of the book 'Spectroscopic coefficients of the p^n, d^n, and f^n configurations' by Nielson and Koster [21] is devoted to tabulating matrix elements in LS coupling. Further efforts must be devoted to converting these wavefunctions to the intermediate coupling case applicable to lanthanide ions. Fortunately, many references tabulate intermediate-coupled matrix elements based on Nielson and Koster's work. Because the electric dipole transitions arise from a small crystal-field perturbation, the matrix elements are not highly dependent on the host material.

These matrix elements are integrals of the dipole operator between the upper and lower wavefunctions of the transition, where the integration takes place over the volume of the atom. The $U^{(\lambda)}$ are the irreducible tensor forms of the dipole operator. Basically, during the transition the atom can be considered an electric dipole oscillating at some frequency whose amplitude is proportional to the value of this matrix element. It is the interaction of this dipole moment with the electric field of the electromagnetic wave that induces the transition. It is analogous to a classical oscillating dipole driven by an external electric field. Quantum mechanically, the situation is more complicated because the parity between the upper and lower electronic states must be considered. In quantum mechanics, electric dipole transitions between electronic states of the same parity are forbidden. This is basically a result of the fact that the expectation value of the position operator $\mathbf{r}$ is odd under reflection, and vanishes for definite parity. The electronic states have wavefunctions described by spherical harmonics, and as such, have the parity of the angular quantum number ℓ. Considering an electronic shell as a whole, the total parity for n electrons is $\wp = (-1)^{\ell_1+\ell_2+\cdots\ell_n}$, therefore an even number of electrons has parity $\wp = 1$ and an odd number of electrons has parity $\wp = -1$. This means that, regardless of the number of electrons, all states in the 4f shell always have definite parity. In free ions, this means that ED transitions within the 4f shell of lanthanide ions are forbidden. However, electric dipole transitions can be forced if opposite parity states from higher lying configurations outside the 4f shell are mixed into the upper state. This is possible when the atom is placed in a noncentrosymmetric perturbing field such as the crystal field of a lattice in which the atom is embedded. This does not happen in a central field because the Hamiltonian is invariant under coordinate inversion, and the states retain definite parity. The odd-order parts of the crystal field, expanded in a series of spherical harmonics, perturb the system and produce mixed parity states between which electric dipole transitions are allowed. This is, in fact, the starting point from which the Judd–Ofelt theory is based.

Table 10. Calculated branching ratios and lifetimes in Ho^{3+} YLF.

Transition	$\bar{\lambda}$ (nm)	S_{ED} (10^{-20} cm^2)	A_{ED} (s^{-1})	A_{MD} (s^{-1})	β	τ_r (ms)	τ_m (ms)
$^5F_2 \rightarrow {}^5F_3$	21 882	0.060	0.00		0.0000		
$^5F_2 \rightarrow {}^5F_4$	3 979	0.255	1.50		0.0004		
$^5F_2 \rightarrow {}^5S_2$	3 758	0.010	0.07		0.0000		
$^5F_2 \rightarrow {}^5F_4$	1 791	0.316	21.30		0.0063		
$^5F_2 \rightarrow {}^5I_4$	1 278	0.164	30.60		0.0090		
$^5F_2 \rightarrow {}^5I_5$	1 011	0.509	191.99		0.0568		
$^5F_2 \rightarrow {}^5I_6$	803	0.734	554.92		0.1641		
$^5F_2 \rightarrow {}^5I_7$	627	0.637	1018.55		0.3011		
$^5F_2 \rightarrow {}^5I_8$	476	0.424	1563.29		0.4622	0.296	
$^5F_3 \rightarrow {}^5F_4$	4 864	0.380	0.84		0.0002		
$^5F_3 \rightarrow {}^5S_2$	4 537	0.008	0.02		0.0000		
$^5F_3 \rightarrow {}^5F_5$	1 950	1.652	61.36		0.0178		
$^5F_3 \rightarrow {}^5I_4$	1 357	1.040	115.54		0.0335		
$^5F_3 \rightarrow {}^5I_5$	1 060	0.520	121.45		0.0352		
$^5F_3 \rightarrow {}^5I_6$	834	0.651	314.11		0.0909		
$^5F_3 \rightarrow {}^5I_7$	646	1.022	1068.40		0.3093		
$^5F_3 \rightarrow {}^5I_8$	487	0.720	1772.28		0.5131	0.290	
$^5F_4 \rightarrow {}^5S_2$	67 568	0.042	0.00		0.0000		
$^5F_4 \rightarrow {}^5F_5$	3 255	0.448	2.72	2.62	0.0008		
$^5F_4 \rightarrow {}^5I_4$	1 882	0.590	19.00		0.0056		
$^5F_4 \rightarrow {}^5I_5$	1 356	1.262	109.28		0.0323		
$^5F_4 \rightarrow {}^5I_6$	1 006	0.928	197.47		0.0584		
$^5F_4 \rightarrow {}^5I_7$	744	0.510	269.47		0.0796		
$^5F_4 \rightarrow {}^5I_8$	541	2.006	2786.17		0.8233	0.295	
$^5S_2 \rightarrow {}^5F_5$	3 420	0.032	0.30		0.0001		
$^5S_2 \rightarrow {}^5I_4$	1 935	0.645	34.30		0.0160		
$^5S_2 \rightarrow {}^5I_5$	1 384	0.230	33.77		0.0158		
$^5S_2 \rightarrow {}^5I_6$	1 022	0.366	134.04		0.0627		
$^5S_2 \rightarrow {}^5I_7$	753	0.852	783.87		0.3667		
$^5S_2 \rightarrow {}^5I_8$	545	0.472	1151.38		0.5386	0.468	0.24
$^5F_5 \rightarrow {}^5I_4$	4 458	0.022	0.04		0.0000		
$^5F_5 \rightarrow {}^5I_5$	2 324	0.411	5.71		0.0032		
$^5F_5 \rightarrow {}^5I_6$	1 457	1.320	75.33		0.0417		
$^5F_5 \rightarrow {}^5I_7$	965	1.656	327.37		0.1813		
$^5F_5 \rightarrow {}^5I_8$	649	2.134	1397.43		0.7738	0.554	0.05
$^5I_4 \rightarrow {}^5I_5$	4 854	2.203	3.83	1.49	0.0474		
$^5I_4 \rightarrow {}^5I_6$	2 164	1.446	30.49		0.3770		
$^5I_4 \rightarrow {}^5I_7$	1 231	0.333	38.59		0.4772		
$^5I_4 \rightarrow {}^5I_8$	759	0.016	7.97		0.0985	12.14	
$^5I_5 \rightarrow {}^5I_6$	3 903	1.621	4.59	3.85	0.0348		
$^5I_5 \rightarrow {}^5I_7$	1 650	1.901	74.48		0.5649		
$^5I_5 \rightarrow {}^5I_8$	900	0.217	52.77		0.4002	7.37	0.02
$^5I_6 \rightarrow {}^5I_7$	2 858	2.269	14.21	8.77	0.0902		
$^5I_6 \rightarrow {}^5I_8$	1 170	1.533	143.31		0.9098	6.01	2.5
$^5I_7 \rightarrow {}^5I_8$	1 981	3.492	57.68	15.41	1.0000	13.68	14.5

The Judd–Ofelt parameters, Ω_λ, consist of odd-order parameters of the crystal field, radial integrals over wavefunctions of the $4f^n$ and perturbing, opposite parity wavefunctions, and energies separating these states in terms of perturbation energy denominators. In principle it

Table 11. Measured and calculated values for the Linestrength in Ho^{3+} LuLF.

Transition (from $^5I_8$)	$\lvert\langle U^{(2)}\rangle\rvert^2$	$\lvert\langle U^{(4)}\rangle\rvert^2$	$\lvert\langle U^{(6)}\rangle\rvert^2$	$\bar{\lambda}$ (nm)	Linestrength (10^{-20} cm^2)	
					Measured	Calculated
$^3K_6 + {}^3F_4$	0.0026	0.1263	0.0073	333	0.2509	0.2980
$^3L_9 + {}^5G_3$	0.0185	0.0052	0.1169	345	0.3004	0.3868
$^3D_2 + {}^3H_6 + {}^5G_5$	0.2155	0.1969	0.1679	361	1.2756	1.0572
$^3K_7 + {}^5G_4$	0.0058	0.0361	0.0697	385	0.3065	0.2342
$^3G_5$	0.0000	0.5338	0.0002	417	1.1195	1.1823
$^5F_1 + {}^5G_6$	1.5201	0.8410	0.1411	450	4.0142	4.0149
$^3K_8$	0.0208	0.0334	0.1535	467	0.2481	0.4238
$^3F_2$	0.0000	0.0000	0.2041	473	0.3751	0.4309
$^3F_3$	0.0000	0.0000	0.3464	486	0.7133	0.7313
$^5F_4 + {}^5S_2$	0.0000	0.2392	0.9339	538	2.4956	2.5013
$^5F_5$	0.0000	0.4250	0.5687	644	2.2018	2.1416
$^5I_5$	0.0000	0.0100	0.0936	897	0.1411	0.2198

is possible to calculate the Judd–Ofelt parameters *ab initio*, but this requires accurate values for the radial integrals and odd crystal-field components, which are not known to a high enough degree of precision. What is usually done is to treat the Judd–Ofelt parameters as a set of phenomenological parameters to be determined from fitting experimental absorption measurements determined in (7) with the theoretical Judd–Ofelt expression in (9). The least squares fitting procedure has been carried out for Ho:GdLF, YLF and LuLF. The results of the fit are shown in tables 7, 9 and 11, respectively. The transition probabilities follow from

$$A(aJ;bJ') = \frac{64\pi^4 e^2}{3h(2J+1)\bar{\lambda}^3}\left[n\left(\frac{n^2+2}{3}\right)^2 S_{\mathrm{ED}}(aJ;bJ') + n^3 S_{\mathrm{MD}}(aJ;bJ')\right] \tag{10}$$

where n is the index of refraction of the solid, and $S_{\mathrm{ED}}(aJ;bJ')$ and $S_{\mathrm{MD}}(aJ;bJ')$ represent the electric and magnetic dipole line strengths. In this equation J represents the total angular momentum of the upper excited state. Electric dipole linestrengths, S_{ED}, were calculated from each excited manifold to all lower lying manifolds using (9) along with the relevant matrix elements and the Judd–Ofelt parameters extracted from the fit. Magnetic dipole linestrengths were calculated in a straightforward way from angular momentum considerations [22]. These values were then converted to intermediate coupling values using the free-ion wavefunctions for triply ionized holmium [23]. The calculation of magnetic dipole linestrengths, S_{MD}, in intermediate coupling has been covered in a previous paper by one of the authors [24]. The radiative lifetimes, τ_{r}, follow from

$$\tau_{\mathrm{r}} = \frac{1}{\sum_{J'} A(J,J')} \tag{11}$$

and the branching ratios, β, follow from

$$\beta_{JJ'} = \frac{A(J,J')}{\sum_{J'} A(J,J')}. \tag{12}$$

The results of these calculations for the first ten manifolds in Ho:GdLF, YLF and LuLF are shown in tables 8, 10 and 12, respectively. In addition, some measured lifetimes at low temperature, 20 K, appear in the last column. Even at very low temperatures, nonradiative quenching of the lifetime occurs, so agreement between the Judd–Ofelt and measured lifetimes are not always expected to be in agreement. This is especially true the smaller is the energy

Table 12. Calculated branching ratios and lifetimes in Ho^{3+} LuLF.

Transition	$\bar{\lambda}$ (nm)	S_{ED} (10^{-20} cm^2)	A_{ED} (s^{-1})	A_{MD} (s^{-1})	β	τ_r (ms)	τ_m (ms)
$^5F_2 \rightarrow {}^5F_3$	21 692	0.064	0.00		0.0000		
$^5F_2 \rightarrow {}^5F_4$	3 976	0.256	1.50		0.0004		
$^5F_2 \rightarrow {}^5S_2$	3 768	0.010	0.07		0.0000		
$^5F_2 \rightarrow {}^5F_4$	1 791	0.321	21.61		0.0063		
$^5F_2 \rightarrow {}^5I_4$	1 277	0.167	31.11		0.0091		
$^5F_2 \rightarrow {}^5I_5$	1 011	0.508	191.75		0.0561		
$^5F_2 \rightarrow {}^5I_6$	803	0.743	561.93		0.1643		
$^5F_2 \rightarrow {}^5I_7$	627	0.641	1024.75		0.2996		
$^5F_2 \rightarrow {}^5I_8$	476	0.431	1587.57		0.4626	0.292	
$^5F_3 \rightarrow {}^5F_4$	4 869	0.390	0.86		0.0002		
$^5F_3 \rightarrow {}^5S_2$	4 560	0.008	0.02		0.0000		
$^5F_3 \rightarrow {}^5F_5$	1 952	1.676	62.12		0.0178		
$^5F_3 \rightarrow {}^5I_4$	1 357	1.051	116.80		0.0335		
$^5F_3 \rightarrow {}^5I_5$	1 060	0.518	121.02		0.0347		
$^5F_3 \rightarrow {}^5I_6$	834	0.657	316.72		0.0908		
$^5F_3 \rightarrow {}^5I_7$	646	1.026	1072.74		0.3075		
$^5F_3 \rightarrow {}^5I_8$	487	0.731	1798.74		0.5155	0.287	
$^5F_4 \rightarrow {}^5S_2$	71 942	0.042	0.00		0.0000		
$^5F_4 \rightarrow {}^5F_5$	3 257	0.462	2.80	2.62	0.0008		
$^5F_4 \rightarrow {}^5I_4$	1 881	0.598	19.27		0.0056		
$^5F_4 \rightarrow {}^5I_5$	1 356	1.276	110.52		0.0324		
$^5F_4 \rightarrow {}^5I_6$	1 007	0.931	197.96		0.0580		
$^5F_4 \rightarrow {}^5I_7$	744	0.509	268.86		0.0788		
$^5F_4 \rightarrow {}^5I_8$	541	2.026	2813.51		0.8244	0.293	
$^5S_2 \rightarrow {}^5F_5$	3 412	0.032	0.30		0.0001		
$^5S_2 \rightarrow {}^5I_4$	1 932	0.653	34.98		0.0161		
$^5S_2 \rightarrow {}^5I_5$	1 382	0.234	34.41		0.0158		
$^5S_2 \rightarrow {}^5I_6$	1 021	0.371	136.08		0.0626		
$^5S_2 \rightarrow {}^5I_7$	752	0.865	797.49		0.3669		
$^5S_2 \rightarrow {}^5I_8$	545	0.479	1170.62		0.5385	0.460	
$^5F_5 \rightarrow {}^5I_4$	4 452	0.022	0.04		0.0000		
$^5F_5 \rightarrow {}^5I_5$	2 322	0.417	5.80		0.0032		
$^5F_5 \rightarrow {}^5I_6$	1 457	1.336	76.23		0.0419		
$^5F_5 \rightarrow {}^5I_7$	965	1.668	329.83		0.1814		
$^5F_5 \rightarrow {}^5I_8$	649	2.147	1406.54		0.7735	0.550	
$^5I_4 \rightarrow {}^5I_5$	4 854	2.234	3.88	1.49	0.0474		
$^5I_4 \rightarrow {}^5I_6$	2 165	1.467	30.88		0.3766		
$^5I_4 \rightarrow {}^5I_7$	1 232	0.338	39.14		0.4774		
$^5I_4 \rightarrow {}^5I_8$	760	0.016	8.08		0.0986	11.98	
$^5I_5 \rightarrow {}^5I_6$	3 908	1.641	4.63	3.85	0.0347		
$^5I_5 \rightarrow {}^5I_7$	1 650	1.930	75.53		0.5654		
$^5I_5 \rightarrow {}^5I_8$	901	0.220	53.44		0.4000	7.27	
$^5I_6 \rightarrow {}^5I_7$	2 857	2.300	14.42	8.77	0.0902		
$^5I_6 \rightarrow {}^5I_8$	1 170	1.556	145.42		0.9098	5.93	
$^5I_7 \rightarrow {}^5I_8$	1 982	3.541	58.46	15.41	1.0000	13.54	14.8

gap to the next lower lying manifold. The gap between the $^5I_7$ and $^5I_8$ is the largest by far. In this case the Judd–Ofelt values and the low temperature lifetime for the $^5I_7$ manifold are in good agreement. Overall, the results are quite good, and within the range of error associated

Table 13. Judd–Ofelt intensity parameters, Ω_λ, and RMS deviation, δ, for Ho:GdLF, Ho:LuLF and Ho:YLF.

Ion:host	Ω_2 (10^{-20} cm^2)	Ω_4 (10^{-20} cm^2)	Ω_6 (10^{-20} cm^2)	δ (10^{-20} cm^2)	Reference
Ho:GdLF	1.289 ± 0.087	2.309 ± 0.097	2.211 ± 0.064	0.117	This study
Ho:LuLF	1.238 ± 0.087	2.214 ± 0.097	2.111 ± 0.064	0.108	This study
Ho:YLF	1.161 ± 0.087	2.224 ± 0.097	2.079 ± 0.064	0.114	This study
Ho:YLF	1.03	2.32	1.93	0.13	[24]
Ho:YLF	1.16	1.62	1.60	—	[25]
Ho:YLF	0.96	2.05	1.43	0.18	[26]

with the Judd–Ofelt theory. Finally, the Judd–Ofelt parameters for this analysis are tabulated along with other sets from the literature for Ho:YLF. These are shown in table 13 along with the intensity parameters for Ho:GdLF and Ho:LuLF. The Judd–Ofelt parameters measured here for Ho:YLF are in reasonable agreement with previous studies. As might be expected the Judd–Ofelt parameters are indeed very similar for Ho:YLF and the isomorphs Ho:LuLF and Ho:GdLF.

6. Summary

The energy levels of Ho^{3+} ions in GdLF, YLF and LuLF have been measured. Crystal-field parameters were varied to determine the best fit between experimental and theoretical energy levels. The energy levels of the first ten manifolds of Ho:GdLF, Ho:YLF and Ho:LuLF have been determined here as well as their crystal-field parameters. In addition, the intensity parameters have been determined from a Judd–Ofelt analysis and used to calculate branching ratios and radiative lifetimes. This paper provides useful information for those doing research involving trivalent Ho ions in the fluoride isomorphs GdLF, YLF and LuLF. A knowledge of the energy levels is an indispensable piece of information when considering a laser ion in a given host material. The energy levels of Ho:GdLF and Ho:LuLF are seen to be very similar to those in Ho:YLF. However, subtle changes resulting from replacing Y with Gd or Lu in the fluoride crystal YLF result in shorter transition wavelengths in GdLF and longer transition wavelengths in LuLF. The energy levels for Ho:LuLF measured here indicate that Ho:LuLF lasers will have a reduced lower laser thermal population than Ho:YLF for improved performance of $^5I_7 \rightarrow {}^5I_8$ lasing at $\sim$2.0 μm compared to YLF. The energy levels for Ho:GdLF measured here indicate that Ho:GdLF lasers will have a larger lower laser level thermal population than Ho:YLF for diminished performance of $^5I_7 \rightarrow {}^5I_8$ lasing at $\sim$2.0 μm compared to YLF. In general, the energy levels measured here and the Judd–Ofelt intensity parameters should be of interest to those in the spectroscopy and laser community doing research with Ho^{3+} ions in $GdLiF_4$ and $LuLiF_4$, the isomorphs of $YLiF_4$.

References

[1] Filer E D, Morrison C A, Barnes N P and Walsh B M 1994 *ASSL Trends Opt. Photon.* **20** 127
[2] Jani M G, Barnes N P, Murray K E, Hart D W, Quarles G J and Castillo V K 1997 *IEEE J. Quantum Electron.* **33** 112
[3] Bensalah A, Shimamura K, Sudesh V, Sato H, Ito K and Fukuda T 2001 *J. Cryst. Growth* **223** 539
[4] Sudesh V, Asai K, Shimamura K and Fukuda T 2001 *Opt. Lett.* **26** 1675
[5] Sudesh V, Shimamura K, Sato H, Bensalah A, Asai K, Machida H, Sarukurac N and Fukuda T 2002 *Recent Res. Dev. Mater. Sci.* **3** 163
[6] Sudesh V, Asai K, Shimamura K and Fukuda T 2002 *IEEE J. Quantum Electron.* **38** 1102

[7] Sudesh V and Asai K 2003 *J. Opt. Soc. Am.* B **20** 1829
[8] Petros M, Yu J, Chen S, Singh U N, Walsh B M, Bai Y and Barnes N P 2003 *Proc. SPIE* **4893** 203
[9] Petros M, Yu J, Singh U N, Walsh B M and Barnes N P 2003 *ASSL Trends Opt. Photon.* **83** 315
[10] Shannon R D 1976 *Acta Crystallogr.* **32** 751
[11] Ranieri I M, Morato S P, Courrol L C, Shihomatsu H M, Bressiani A H A and Moraes N M P 2000 *J. Cryst. Growth* **209** 906
[12] Ranieri I M, Shimamura K, Nakano K, Fujita T, Courrol L C, Morato S P and Fukuda T 2000 *J. Cryst. Growth* **217** 145
[13] Karayanis N, Wortman D E and Jenssen H P 1976 *J. Phys. Chem. Solids* **37** 675
[14] Gifeisman Sh N, Tkachuk A M and Prizmak V V 1978 *Opt. Spectrosc.* **44** 68
[15] Pourat B, Pilwa B and Kahle H G 1991 *J. Phys.: Condens. Matter* **3** 6069
[16] Morrison C A and Leavitt R P 1979 *J. Chem. Phys.* **71** 2366
[17] Leavitt R P and Morrison C A 1980 *J. Chem. Phys.* **73** 749
[18] Carnall W T, Fields P R and Rajnak K 1968 *J. Chem. Phys.* **49** 4424
[19] Judd B R 1962 *Phys. Rev.* **127** 750
[20] Ofelt G S 1962 *J. Chem. Phys.* **37** 511
[21] Nielson C W and Koster G F 1963 *Spectroscopic Coefficients of the p^n, d^n and f^n Configuration* (Cambridge, MA: MIT Press)
[22] Shortly G H 1940 *Phys. Rev.* **57** 225
[23] Rajnak K and Krupke W J 1967 *J. Chem. Phys.* **46** 3532
[24] Walsh B M, Barnes N P and Di Bartolo B 1998 *J. Appl. Phys.* **83** 2772
[25] Tkachuk A M, Khilko A V and Petrov M V 1985 *Opt. Spectrosc.* **58** 55
[26] Li C, Guyot Y, Linares C, Moncorge R and Joubert M F 1993 *ASSL Proc.* **15** 91